Accurate Gas-phase Structure of $para$-Dioxane by Fs Raman Rotational Coherence Spectroscopy and Ab Initio Calculations

Takuya Den, Samuel Menzi, Hans-Martin Frey and Samuel Leutwyler*

Departement für Chemie und Biochemie, Universität Bern,

Freiestrasse 3, CH-3000 Bern 9, Switzerland

(Dated: July 13, 2017)

Abstract

p-Dioxane is non-polar, hence its rotational constants cannot be determined by microwave RCS spectroscopy. We perform high-resolution gas-phase rotational spectroscopy of $para$-dioxane-h_8 and $-d_8$ using femtosecond time-resolved Raman rotational coherence spectroscopy (RCS) in a gas cell at $T = 293$ K and in a pulsed supersonic jet at $T \sim 130$ K. The inertial tensor of p-dioxane-h_8 is strongly asymmetric, leading to a large number of asymmetry transients in its RCS spectrum. In contrast, the d_8-isotopomer is a near-oblate symmetric top that exhibits a much more regular RCS spectrum with few asymmetry transients. Fitting the fs Raman RCS transients of p-dioxane-h_8 to an asymmetric-top model yields the ground-state rotational constants $A_0 = 5084.4(5)$ MHz, $B_0 = 4684(1)$ MHz, $C_0 = 2744.7(8)$ MHz and $(A_0 + B_0)/2 = 4884.5(7)$ MHz ($\pm 1\sigma$). The analogous values for p-dioxane-d_8 are $A_0 = 4083(2)$ MHz, $B_0 = 3925(4)$ MHz, $C_0 = 2347.1(6)$ MHz and $(A_0 + B_0)/2 = 4002.4(6)$ MHz. We determine the molecular structure with a semi-experimental approach involving the highly correlated CCSD(T) method and the cc-pCVXZ basis set series from double- to quadruple-zeta (X=D, T, Q). Combining the calculated vibrationally-averaged rotational constants $A_0^{calc}(X), B_0^{calc}(X), C_0^{calc}(X)$ for increasing basis-set size X with non-linear extrapolation to the experimental constants $A_0^{exp}, B_0^{exp}, C_0^{exp}$ allows to determine the equilibrium ground state structure of p-dioxane. For instance, the equilibrium C-C and C-O bond lengths are r_e(CC)$= 1.5135(3)$Å and r_e(CO)$= 1.4168(4)$ Å, and the four axial C-H bond lengths are 0.008 Å longer than the four equatorial ones. The latter is ascribed to the trans-effect (anomeric effect), i.e., the partial delocalization of the electron lone-pairs on the O atoms that are oriented *trans* relative to the axial CH bonds.

Keywords: Dioxane, rotational coherence, bond length, time resolved Raman scattering, degenerate four wave mixing, asymmetric rotor, molecular beam

I. INTRODUCTION

p-Dioxane is a common solvent in many industrial and laboratory applications due to its low polarity and high boiling point. Its six-membered ring can assume three locally stable conformations denoted chair, boat and twist-boat, which are analogous to those of cyclohexane.[2,3,5–7] Since p-dioxane has no dipole moment, its rotational constants are not accessible by microwave spectroscopic techniques. Rotational coherence spectroscopy (RCS) is a time-domain spectroscopic method,[8–10] which in its Raman variant can deliver accurate rotational constants of non-polar molecules.[11–21]

Brown et. al. measured the ground state rotational constants of jet-cooled p-dioxane-h_8 using high-resolution infrared (IR) diode-laser absorption spectroscopy and assigned the rotational spectrum based on an asymmetric-top model employing Watson's A-reduced Hamiltonian representation.[4] Given the $\sim$ 10 K temperature in their jet expansion, only low-lying rotational levels were populated, which precluded fitting the centrifugal distortion constants.[4] Their rotational constants[4] $A_0 = 5083.2(3)$ MHz, $B_0 = 4684.4(3)$ MHz, $C_0 = 2743.6(1)$ MHz and $(A_0 + B_0)/2 = 4883.8(3)$ MHz correspond to a rigid asymmetric-top model with centrifugal distortion constants set to zero.

In this work we study the gas-phase rotational motion of p-dioxane$-h_8$ and of its fully deuterated d_8-isotopomer, using time-resolved femtosecond (fs) Raman RCS spectroscopy, detected by degenerate four-wave mixing (DFWM) both in a supersonic jet and in a room-temperature gas cell. We analyzed the RCS transients in terms of a *non*-rigid asymmetric top model taking the centrifugal distortion constants from highly correlated CCSD(T) calculations. Since we measure at two temperatures (130 K and 293 K, see below), which are much higher than in ref. 4, it was mandatory to include the effects of centrifugal distortion in the fit. Thus, while the p-dioxane$-h_8$ rotational constants measured by IR laser spectroscopy[4] are expected to differ slightly from those determined here, they constitute a valuable data set for cross-checking and validating our fs Raman RCS experiment and asymmetric-top RCS fitting program. We also combined the rotational constants with results of quantum chemical calculations at CCSD(T) level and used a semi-experimental procedure based on basis-set extrapolation to obtain the equilibrium structure of p-dioxane, providing accurate bond lengths and angles.[30–36]

In a gas-phase electron-diffraction (GED) study at room temperature, Davis and Hassel found that p-dioxane exists exclusively in the chair form.[2] They reported the $298K$ vibrationally averaged

bond lengths r_a(C-C), r_a(C-O) and r_a(C-H) (averaged over the equatorial and axial C-H bonds) and the vibrationally averaged C-C-O and C-O-C bond angles.[2] In a later reinvestigation of the p-dioxane structure using GED, Farger et. al. determined all ten structure parameters of the chair form, including the two C-C-H and H-C-H bond angles and the "flap" angle of the six-ring (i.e., the tilt angle of the C-O-C plane relative to that of the four carbon atoms).[7] They confirmed the previous finding[2] that the GED pattern is explained by the chair form alone.[7] Based on the B3LYP/cc-pVTZ calculated ΔE and ΔG^0_{298K} values they estimated the ratio of the chair relative to the next higher twist-boat conformer as $10'000 : 1$ at 298 K. Caminati et. al. performed a microwave study on the p-dioxane·water complex produced in a supersonic jet expansion.[22] In their analysis they employed the p-dioxane r_α structure of Davis and Hassel [2] and determined the structure parameters of the complex, but did not report new information on the p-dioxane moiety.[22]

The chair $\leftrightarrow$ chair inversion process in dioxane was investigated by two ^{1}H NMR spectroscopic studies, in which the barrier for the ring-inversion was determined as $\Delta G^\ddagger = 9.4$ kcal/mol at 176 K and as 9.7 kcal/mol at 143 K.[3,5] An X-ray diffraction investigation over the temperature range $133 - 285$ K showed that the chair form is also the dominant conformation in the solid state.[6]

Pickett and Strauss investigated the potential energy surface and the chair$\leftrightarrow$chair inversion process in dioxane and in related oxanes, using a potential derived from vibrational and geometrical data.[23] They constructed a detailed conformational energy map which they used to estimate the chair$\leftrightarrow$chair transition state energy as 11 kcal/mol.[23] Chapman et. al. performed a conformational analysis of p-dioxane at the ab-initio HF/6-31G*, B3LYP/6-31* and MP2/6-31* levels, and characterized ten stationary points as minima or transition structures.[24] Based on a vibrational analysis they proposed a detailed inversion mechanism chair $\leftrightarrow$ [1,4 half-chair] $\leftrightarrow$ 1,4 twist-boat $\leftrightarrow$ [1,4 half-chair] $\leftrightarrow$ chair, with a 1,4-half-chair barrier energy of 12.8 kcal/mol at the MP2/6-31* level.[24]

We have measured the Raman RCS transients of p-dioxane-h_8 and -d_8 in order to obtain accurate ground-state rotational constants. The structure of p-dioxane is analogous to those of the isoelectronic molecules cyclohexane (C_6H_{12})[25–28] and piperidine ($C_5H_{11}N$).[29,30] While cyclohexane is an oblate symmetric-top molecule that is characterized by an asymmetry parameter $\kappa \equiv (2B_0 - A_0 - C_0)/(A_0 - C_0) = +1.000$,[25–28] piperidine is a near-oblate asymmetric-top molecule with $\kappa = +0.91$ for its parent isotopomer.[30] Replacing both methylene groups of cyclohexane by O atoms increases the asymmetry of p-dioxane, rendering it a strongly asymmetric top with $\kappa = +0.656$, see below. The increase of asymmetry gives rise to *asymmetry transients* in the Raman RCS spectrum of p-dioxane, which are not observable for cyclohexane,[27,28] and which

give detailed information on the rotational constants of p-dioxane. Interestingly, p-dioxane-d_8 has a more symmetric mass distribution than the h_8-isotopomer, making p-dioxane-d_8 a near-oblate asymmetric top. Systematically changing κ from $+0.66$ to $+1.0$ for these structurally related molecules allows to study the influence of the inertial tensor on the Raman RCS spectrum. A further point is that the intensity of rotational Raman transitions and thus of the Raman RCS spectrum depends on the anisotropy of the molecular polarizability tensor $\widehat{\alpha}$, which is dominantly an electronic property. While the eightfold H/D substitution of p-dioxane-h_8 strongly modifies the inertial tensor of p-dioxane, it has no effect on the polarizability tensor, leading to a rotation of $\widehat{\alpha}$ with respect to the inertial frame.

The detailed simulation of the asymmetric-top Raman RCS transients of p-dioxane$-h_8$ and $-d_8$ allows to fit the experimental transients and thereby determine two sets of rotational constants $\{A_0, B_0, C_0\}$. Given that p-dioxane has ten independent structure parameters, six rotational constants do not suffice to determine the equilibrium molecular structure. However, combining the experimental rotational constants with coupled-cluster CCSD(T) calculations based on a systematic series of basis sets (the Dunning cc-pCVXZ series with X=D, T and Q) allows to determine the semi-experimental r_e structure[30–36] of p-dioxane using a non-linear basis-set extrapolation.

II. EXPERIMENTAL METHODS

The experimental setup used to record fs-DFWM-RCS transients has been described previously.[27,28] In short, a 1 kHz repetition rate amplified Ti:sapphire laser system delivers pulses of ~ 75 fs which are split into three beams of equal energy ($10 - 100$ μJ/pulse per beam), which act as the Raman pump and dump pulses, followed by the time-delayed probe pulse. The three beams are parallelized and focused by a $f = 1000$ mm achromatic lens into the probe volume in a folded BOXCARS arrangement.[37] Measurements were performed in a gas cell at $T = 293$ K[36,38] and in a pulsed supersonic jet, employing Ar as a carrier gas.[28,39]

For the supersonic-jet measurements p-dioxane-h_8 was heated to 80° C, equivalent to a partial pressure of $p = 500$ mbar;[40] the vapor was entrained in Ar carrier gas at a backing pressure of 1000 mbar. The gas mixture was expanded through a pulsed 0.6 mm diameter nozzle (333 Hz repetition rate) into a ~ 0.1 mbar vacuum that is maintained by a Roots blower/ rotary-vane vacuum pump combination. The RCS signal was generated in the overlap volume of the pump, dump and probe laser beams within the core of the jet expansion ~ 2 mm downstream of the nozzle

orifice. The pump, dump and probe pulses were blocked, while the coherently generated RCS signal beam was recollimated, spatially filtered and detected by a thermoelectrically cooled GaAs photomultiplier. The transients were obtained by scanning the delay time between the pump/dump and the probe pulses in steps of ∼20 fs. Due to the large quantity ($\sim 300 - 500$ ml) of p-dioxane needed per experiment, jet measurements of p-dioxane-d_8 were not feasible.

III. COMPUTATIONAL METHODS AND RESULTS

Quantum-chemical calculations and optimizations of the equilibrium (r_e) geometries of p-dioxane chair-h_8 and twist-chair-h_8 were performed with the coupled-cluster approach using single and double excitations augmented by a perturbational estimate of connected triple excitations, CCSD(T). All electrons were correlated. The structures were optimized using the correlation-consistent polarized core-valence double-, triple- and quadruple-zeta basis sets cc-pCVDZ, cc-pCVTZ and cc-pCVQZ.[41] It has been shown that the inclusion of high-order electron correlation and of core-valence correlation is important to achieve highly accurate structures and rotational constants.[43–47]

The anharmonic vibrational frequencies, vibrationally averaged rotational constants A_v, B_v and C_v and the molecular polarizability tensor were calculated for both conformers as well as for p-dioxane-d_8 (chair) at the CCSD(T)/cc-pCVDZ level, using analytical second-derivative techniques.[48,49] All calculations were carried out with the CFOUR program.[50]

The CCSD(T)/cc-pCVQZ calculated structure of the chair isomer is shown in Figure 1. The Z-matrices and the CCSD(T)/cc-pCVXZ optimized structure parameters of the chair conformer are listed in Table S2 to S5 of the supplemental information (SI), those of the twist-chair conformer in Tables S6 to S8 of the SI. The equilibrium rotational constants A_e, B_e, C_e and $v = 0$ vibrationally averaged rotational constants A_0, B_0, C_0 and the elements of the electronic polarizability tensor $\widehat{\alpha}$ of the chair and twist-boat conformers of p-dioxane-h_8 and -d_8 are reported in Table I.

IV. RAMAN RCS SPECTROSCOPY OF ASYMMETRIC-TOP MOLECULES

A. Modeling the RCS signal

The RCS signal $I(t)$ is proportional to the square modulus of its time-dependent third-order susceptibility $\chi^{(3)}(t)$ and can be written as:[51–53]

$$I(t) = \int_{-\infty}^{\infty} G(\tau)|\chi^{(3)}(t-\tau)|^2 d\tau \tag{1}$$

The experimental apparatus function $G(t)$ is determined by the triple convolution of the fs Raman pump, dump and probe pulses and was measured prior to every RCS experiment using the time-domain Kerr-effect signal of Ar gas in the gas cell or in the supersonic jet at time zero. $G(t)$ can be modeled by a Gaussian of 140 fs full width at half maximum (FWHM); the center of $G(t)$ was also used to establish time-zero of the RCS experiment. The $\chi^{(3)}(t)$ associated with non-resonant rotational Raman excitation of asymmetric-top rotational states is given by

$$\chi^{(3)}(t) \sim C + \sum_{\Gamma<\Gamma'} c_{\Gamma,\Gamma'} \sin[(E_{\Gamma'} - E_{\Gamma})t/\hbar] \tag{2}$$

where $\Gamma \equiv J_\tau$ and $\Gamma' \equiv J'_{\tau'}$ denote the asymmetric-top rotational levels and E_Γ and $E_{\Gamma'}$ are their respective rotational energies. In eqn.(2) the modulation amplitude $c_{\Gamma,\Gamma'}$ is a product of (1) the ground- and excited state population differences $e^{\frac{-E_{\Gamma'}}{k_b T}} - e^{\frac{-E_{\Gamma}}{k_b T}}$, (2) the fractional vibrational population of the vibrational level v, p_v, (3) the nuclear-spin statistical weight of the rotational level $g_{ns,\Gamma}$, and (4) the rotational Raman transition probabilities $b_{\Gamma,\Gamma'}$. For asymmetric-top molecules, the latter have to be calculated numerically, using the wave functions described in eqn.(4) below. For linear and symmetric-top molecules rotational the Raman transition probabilities can be calculated analytically and are known as Placzek-Teller factors (coefficients).[42,54]

The empirical parameter C accounts for slight distortions of the RCS signal which may arise from stray light that temporally coincides with the probe pulse. In practice this is only important for very weak RCS signals.

B. Energy levels of asymmetric-top molecules

For the calculation of the rotational energy levels J_τ we choose Watson's A-reduced Hamiltonian including the first-order (quartic) Watson centrifugal distortion constants Δ_J, Δ_K, Δ_{JK}, δ_J and δ_K:[55,56]

$$\begin{aligned}\hat{H}_{rot} =& A\hat{J}_z + \frac{1}{2}(B+C)(\hat{J}^2 - \hat{J}_z^2) + \frac{1}{4}(B-C)(\hat{J}_+^2 + \hat{J}_-^2) \\ & - \Delta_J \hat{J}^4 - \Delta_{JK}\hat{J}_z^2 - \Delta_K \hat{J}_z^4 - \frac{1}{2}[\delta_J \hat{J}^2 + \delta_k \hat{J}_z^2, \hat{J}_+^2 + \hat{J}_-^2]\end{aligned} \tag{3}$$

The calculated equilibrium rotational constants A_e, B_e, C_e, the $v = 0$ vibrationally averaged constants A_0, B_0, C_0 and the centrifugal distortion constants are listed in Table I.

The asymmetric-top energy levels are determined by diagonalization of the asymmetric-top Hamiltonian in a symmetric-top basis.[55,57] Asymmetric-top eigenfunctions $|\Gamma M\rangle$ can be expressed as linear combinations of symmetric-top eigenfunctions $|JKM\rangle$:

$$|\Gamma M\rangle = |J\tau M\rangle = \sum_{K=-J}^{J} a(\Gamma, K)|JKM\rangle \tag{4}$$

where $\tau = K_{-1} - K_{+1}$ is the difference of the corresponding prolate and oblate symmetric-top state K quantum numbers. The subscripts -1 and $+1$ refer to $\kappa = (2B - A - C)/(A - C)$, where $\kappa = -1$ corresponds to the prolate symmetric-top and $\kappa = +1.0$ to the oblate symmetric-top limit.[55,57] $K = J, J-1..., -J$ denotes the projection of the total angular momentum J on the major molecule-fixed principal axis, which for p-dioxane is the c-axis, see also Figure 1. For p-dioxane-h_8 the CCSD(T)/cc-pCVQZ calculations predict $\kappa = 0.656$, corresponding to a strongly asymmetric top, see Figure S1. In contrast, p-dioxane-d_8 is much closer to the oblate-top limit with a calculated $\kappa = +0.823$, as shown in Figure S1 and given in Table I.

The rotational energy levels of asymmetric-top molecules lie between the prolate and oblate limits, as shown in Figure S1. In contrast to symmetric-tops, asymmetric-top states are not degenerate for J-states with the same absolute K value. In fact K is not a good quantum number for asymmetric-tops, instead states are specified by J and $\tau = K_{-1} - K_{+1}$.[55,57] However, for molecules that are only slightly asymmetric, K_{+1} and K_{-1} are still approximately good quantum numbers. The rotational Raman selection rules that are discussed below are those for an oblate asymmetric top with $K \sim K_{+1}$.

C. Rotational Raman selection rules and Raman intensities for asymmetric tops

The rotational Raman selection rules between levels $|\Gamma M\rangle$ and $|\Gamma' M'\rangle$ that contribute to the RCS signal (see eqn. 2) arise from the rotational Raman transition moment $\langle \Gamma' M' | \widehat{\alpha} | \Gamma M \rangle$, where $\widehat{\alpha}$ is the 3x3 molecular polarizability tensor. It is defined in the molecule-fixed axis system whose origin is at the molecular center of mass and whose axes are the principal axes $\{a, b, c\}$ of the inertial tensor.[58,59]

The molecular polarizability tensor is an electronic property, so the principal axes of $\widehat{\alpha}$ need not coincide with those of the inertial tensor, which is dominantly a nuclear-framework property. Given the C_{2h} symmetry of p-dioxane-h_8 and p-dioxane-d_8, one axis of $\widehat{\alpha}$ coincides with the b axis of the inertial tensor, the other two axes of $\widehat{\alpha}$ lie in the σ_h symmetry plane that contains the a and c inertial axes, see Figure 1. Since the two axes of $\widehat{\alpha}$ that lie in this plane may be tilted with respect to a and c, an off-diagonal element arises, which is calculated to be $\alpha_{ac} = 1.10$ bohr^3. The CCSD(T)/cc-pCVDZ calculated elements of $\widehat{\alpha}$ are given in part 3 of Table I. With our choice of the molecule-fixed coordinate system for p-dioxane-h_8 we obtain $\alpha_{zz} = \alpha_{cc}$, $\alpha_{yy} = \alpha_{aa}$ and $\alpha_{xx} = \alpha_{bb}$.

A detailed derivation of Raman selection rules for symmetric-top molecules is given in ref. 60. The analogous procedure for finding non-zero values of the rotational Raman transition moment can be applied to asymmetric-top states, as these can be written as a superposition of symmetric-top states, see eqn. 4. Rotational Raman transition moment integrals are best dealt with by decomposing $\widehat{\alpha}$ into irreducible spherical polarizability tensor components, $\alpha_k^{(j)}$, and then using angular momentum coupling rules.[60] The $\alpha_k^{(j)}$ can be regarded as angular momentum states $|J = j, K = k\rangle$ where k runs from $-j$ to $+j$. For p-dioxane only the $\alpha_k^{(2)}$ tensor components contribute to the RCS signal. Each element in $\alpha_k^{(2)}$ can be constructed as a linear combination of the molecular Cartesian polarizability tensor components as shown in Table II. The calculated irreducible spherical tensor components $\alpha_{(0)}^{(2)}$, $\alpha_{(1)}^{(2)}$ and $\alpha_{(2)}^{(2)}$ are given in part III of Table I. The dependence of the allowed changes in K quantum number on the molecular polarizability tensor components allows deeper insight into the simulated RCS transient:[61] For example, if one is interested only in coherences with $\Delta J = 1, 2$ and $\Delta K = 0$ the molecular polarizability is set to values such that $\alpha_{xx} = \alpha_{yy} \neq \alpha_{zz}$ and $\alpha_{off-diagonal} = 0$.[61]

D. Rotational Raman transient types

Raman RCS transients are characterized by recurring features which are a manifestation of regularities in the structure of the rotational energy levels. Regular frequency spacings occur for (rigid) symmetric-top molecules with rotational energies given by $E(J,K) = BJ(J+1) + (C - B)K^2$ for an oblate symmetric top.[10] Felker and co-workers have shown that even for asymmetric molecules, significant subsets of the rotational levels can retain sufficiently regular frequency spacings as to yield rotational recurrences.[8,10,62] These subsets produce transients that are characterized by their recurrence time. Transients are named either by their main contributing coherences (J-type and K-type) or by the rotational constants about which they convey information (A-type and C-type). The relevant transient types for p-dioxane are listed in Table S1; some corresponding rotational transitions are indicated in Figure S1.[10,55] Note that a rotational transition specified by a specific ΔJ and ΔK is not bijectively associated with a single transient type; for instance, rotational transitions with $\Delta J = 2, \Delta K_{-1} = 0$ contribute to both J-type as well as C-type transients.

The relative intensity of transient types with different $|\Delta K|$ values is largely determined by the magnitude of the irreducible spherical polarizability tensor components $\alpha_k^{(2)}$ that promote the contributing rotational transitions. The RCS signal is proportional to the fourth power of $\alpha_k^{(2)}$ thus the intensity of J-type transients is proportional to $|\alpha_{(0)}^{(2)}|^4$ whereas the intensity of K-type, A-type and C-type transients is proportional to $|\alpha_{(2)}^{(2)}|^4$. For both p-dioxane-h_8 and p-dioxane-d_8 J-, A-, C- and K-type transients are expected.

E. Fitting procedure and data analysis

The asymmetric-top RCS transients are calculated via eqns.(1) and (2) using an IDL program (RSI, Inc.); the simulated transient $I_{calc}(t)$ is then fitted to the experimental RCS transient $I_{exp}(t)$ using a Levenberg-Marquardt nonlinear least-squares fit.[28,34–36,61] The starting values of A_0, B_0, C_0 in the fit were taken from the CCSD(T)/cc-pCVQZ calculations, see Table I. The A-reduced centrifugal distortion constants and the α_{aa}, α_{cc} and α_{bc} components of the molecular polarizability tensor were fixed to their CCSD(T)/cc-pCVDZ calculated values (see Table I) and were not fitted. The polarizability tensor component α_{bb} was fitted to the experimental transient to balance the relative intensity of $\Delta K = 0$ and $\Delta K = 2$ transitions.

The number of rotational levels to be considered in the simulation is determined by the cu-

mulative rotational level population at the experimental temperature T and the bandwidth of the fs laser pulse, which limits the highest Raman rotational transition frequencies that can be driven and that contribute to the RCS signal. We considered a cumulative rotational population of $\geq 99\%$ at $T = 293$ K, which corresponds to rotational levels with $J = 0 - 150$. Assuming the oblate symmetric-top limit for p-dioxane and the largest possible quantum-number change $\Delta J = 2/\Delta K = 2$, one obtains $\Delta\nu_{J,K} = 4BJ + 4(A-B)K = 4AJ$, where for the second step we set $K = J$ since we are only interested in the highest transition frequency. The highest rotational level that can be excited within the $BW = 5.6$ THz bandwidth of our of our fs laser system is $J_{max} = BW/4A = 5600GHz/4 \cdot 5.1GHz \sim 270$. This is considerably smaller than the $J = 150$ upper limit considered, so the laser bandwidth is sufficiently large to drive all possible Raman rotational transitions.

In the gas-cell measurements at $T = 293$ K a number of low-lying thermally excited vibrational levels contribute to the RCS signal, see Table III. The v-dependent rotational constants A_v, B_v and C_v can be expressed in terms of the vibration-rotation coupling constants α_v^A, α_v^B, and α_v^C, e.g., for A_v:[63]

$$A_v = A_\mathrm{e} - \sum_{i=1}^{3N-6} \alpha_i^A \left(v_i + 1/2\right) \tag{5}$$

where A_e is the rotational constant associated with the rigid equilibrium structure, the $\alpha_i^{A,B,C}$ are the vibration-rotation interaction constants associated with each of the 36 vibrational modes of p-dioxane, and $v_i = 0, 1, 2, ...$ is the quantum number of the i-th vibrational mode. The vibrational-averaging corrections for the vibrational zero-point level $v = 0$ are denoted $\Delta_{A,B,C}$, e.g., for Δ_A:

$$\Delta_A = A_0 - A_\mathrm{e} = -\frac{1}{2} \sum_{i}^{3N-6} \alpha_i^A \tag{6}$$

The vibrational averaging corrections will be discussed in more detail in section VI.

The thermally populated vibrational levels of p-dioxane-h_8 and -d_8 are ν_7, ν_8, ν_9, ν_{10}, ν_{11}, ν_{12}, $2\nu_7$, $2\nu_8$ and ν_7+ν_8. They account cumulatively for $>$ 99% of the total RCS signal for p-dioxane-h_8 and for $>$ 97% of the RCS signal for p-dioxane-d_8, as can be seen from Table III. The CCSD(T)/cc-pCVDZ calculated rotation-vibration coupling constants for ν_7 to ν_{12} are also given in Table III. The corresponding A_v, B_v, C_v constants were calculated via eqn.(6) and the fractional contributions of these levels to $\chi^{(3)}$ and to the RCS signal were included in the simulated transients and in the fits. The fit parameters in the simulations of the room-temperature gas-cell transients

were A_0, B_0 and C_0, $\alpha_{bb} = \alpha_{xx}$ (see Table II) and the empirical signal distortion parameter C, see eqn.(2).

In the supersonic-jet RCS transient only J-type transients could be observed, in contrast to the room-temperature gas cell transient. The supersonic-jet transient was fitted with the parameters A_0, B_0 and C_0, the rotational temperature T_{rot} and the parameter C; the polarizability tensor component α_{bb} was fixed to its CCSD(T)/cc-pCVDZ calculated value. We initially included the above-mentioned vibrationally excited levels in the fit, but found that these do not contribute significantly to the RCS signal at the supersonic-jet temperature. We thus assumed the vibrational temperature T_{vib} to be equal to the rotational temperature T_{rot}, $T_{vib} \sim T_{rot} = 130 \pm 10$ K. This is in agreement with the calculated vibrational populations in Table III.

V. RESULTS AND DISCUSSION

A. Transient analysis

p-Dioxane-h_8: An overview of the gas-cell transient for delay time $\Delta t = 0 - 650$ ps is shown in Figure 2(a). The transient length is relatively short because of the small anisotropy of the molecular polarizability tensor of p-dioxane, see also Table I. As noted above the RCS signal is proportional to the fourth power of the irreducible spherical polarizability components $\alpha^{(2)}_{(0)}$ and $\alpha^{(2)}_{(2)}$. For p-difluorobenzene[61] we calculated that $\alpha^{(2)}_{(0)} = 19.0$ bohr^3 whereas for p-dioxane-h_8 $\alpha^{(2)}_{(0)}$ is only 4.4 bohr^3. This translates to a decrease of RCS signal intensity by a factor of ~ 250 at equal gas-phase density (pressure). Compared to symmetric-top molecules, the RCS transient decays much faster with increasing Δt because of the relatively large asymmetry of p-dioxane-h_8 ($\kappa = 0.658$). Despite the asymmetry, the RCS transient of p-dioxane-h_8 appears rather simple, being dominated by J-type features. Only a close-up view, which is shown in Figure 3, reveals the fine structure that substantiates the asymmetry of the molecule. Comparison to the gas-cell Raman RCS transient of p-dioxane-d_8 in Figure 2(b) shows that the larger $\kappa = +0.890$ of the perdeuterated compound increases the observable time duration of the RCS transient by a factor of 1.5.

Figure 3(a) compares the experimental transient of p-dioxane-h_8 to the simulated sub-transients shown in panels (b)-(f), which correspond to coherences for specific ΔJ and ΔK values. This procedure[61] emphasizes the signal contributions from different coherences and allows to assign

even small signals to specific transient types. Since asymmetric-top states are eigenfunctions of the total angular momentum J, see eqn. 4, one can restrict ΔJ to a subset of transitions as outlined in section B.3: The coherences for ΔK transitions are selected by setting specific values for the polarizability tensor elements. Combining ΔJ and ΔK restrictions allows to simulate five sub-transients with ΔJ=0/ΔK=2, ΔJ=1/ΔK=0, ΔJ=1/ΔK=2, ΔJ=2/ΔK=0 and ΔJ=2/ΔK=2. Note, however, that changes of the K_{-1} or K_1 quantum numbers cannot be selected. In addition to the intense J-type progression, which occurs at multiples of $\Delta t = 51$ ps, we can assign C-type ($\Delta t = 91$ ps), A-type ($\Delta t = 49$ ps) and K-type ($\Delta t = 118$ ps) coherences.

The summation of the different $\Delta J/\Delta K$ contributions to $\chi^{(3)}$ in eqn.(2) gives rise to interferences between different coherences, which strongly affects the relative intensities of the sub-transients in $I(t)$. Thus the total RCS signal in Figure 3(a) is not obtained by adding the individual sub-transients shown in panels (b)-(f), but by first coherently adding all $\Delta J/\Delta K$ sub-transient amplitudes to obtain $\chi^{(3)}(t)$ - see eqn.(2) - and then modulus-squaring the result to obtain the RCS signal, see eqn.(1). Note also that collisional dephasing effects become important over the 400 ps delay time of the gas-cell RCS transient in Figure 3(a); these effects were not included for the sub-transient analysis.

Twist-boat conformer: We also searched for signatures of the twist-boat-conformer of p-dioxane-h_8. In Figure 4 we compare the experimental room-temperature gas-cell Raman RCS transient to that which we calculate for the cc-pCVTZ optimized twist-boat conformer. Even the most intense predicted signal of the twist-boat predicted at $\Delta t = 193$ ps is not observed. This confirms the result of Hedberg et. al. who were unable to observe the twist-boat conformer.[7]

p-Dioxane-d_8: As discussed above, with $\kappa = 0.890$ p-dioxane-d_8 is much closer to the oblate symmetric-top limit than the h_8-isotopomer. Therefore the rotational level structure of p-dioxane-d_8 has many more close level coincidences than the h_8-isotopomer, which in turn increases the time-delay over which we can observed recurrences with a sufficiently high S/N ratio to $\Delta t = 0 - 900$ ps, as shown in Figure 2(b). The closeness to the oblate symmetric-top case renders the p-dioxane-d_8 transient rather simple, with a dominant J-type progression. At large magnification three additional C-type recurrences are observed at $\Delta t = 320$ ps, $\Delta t = 430$ ps and $\Delta t = 745$ ps. In this case, sub-transient decomposition was not necessary for the assignments.

B. Rotational constants

The complete experimental gas-cell RCS transient of p-dioxane-h_8 at $T = 293$ K is shown in the top panel of Figure 5. Magnified sections of the experimental data are compared to the calculated transients in the 16 following sub-panels. The $v = 0$ vibrational ground state dominates the RCS signal at room temperature (82.7 % of the signal, see Table III). Nevertheless, the transient is strongly influenced by the rotational constants of the thermally populated vibrational states, especially ν_7 (6.3 %) and ν_8 (5.6 %).

As an illustration of the contributions from the thermally populated vibrations to $\chi^{(3)}(t)$, Figure 6 shows a section of the RCS signal with a large A-type transient at 542 ps and a small C-type transient at 547 ps. Since the rotational constants of the excited vibrational levels differ from those of the $v = 0$ level by their respective vibration-rotation coupling constants, see eqns.(5), (6) and Table III), they produce coherences that are slightly time-shifted with respect to the v=0 level, as indicated for the A-type transients by the vertical arrows in Figure 6(a)-(g). These shifts reflect the change of the A_v rotational constant, as is expected for A-type transients. We construct the total $\chi^{(3)}(t)$ in Figure 6(h) by summing traces (a)-(g) for all thermally populated vibrational fundamentals, including additional overtone and combination levels, as listed in Figure 6. The relative population of these levels at $T = 293$ K and respective $\alpha_v^{A,B,C}$ values are given in Table III. The simulated $I(t)$ in Figure 6(i) is obtained from $\chi^{(3)}(t)$ via eqn.(1) and is fitted to the observed $I(t)$ is shown in Figure 6(i). The fit not only involves the rotational level eigenenergies (as is typical for microwave spectroscopy) but also the rotational Raman transition intensities, which are based on the rotational wave functions, see eqn.(4).

We performed analogous fits for all 16 delay-time windows in Figure 5 and averaged the resulting rotational constants, giving $A_0 = 5084.4(5)$ MHz, $B_0 = 4684(1)$ MHz, $C_0 = 2744.7(8)$ MHz and $(A_0 + B_0)/2 = 4884.5(7)$ MHz, with $\pm 1\sigma$ uncertainty given in parentheses, see Table IV. As Table S1 shows, the most intense J-type transients only give information on $(A_0 + B_0)/2$; on the other hand the weak asymmetry transients allow to fit all three rotational constants even without relying on J-type transients. This demonstrates that the presence of asymmetry transients is much more important than large signal intensities when it comes to the determination of rotational constants.

The Raman RCS rotational constants of p-dioxane-h_8 agree nicely with the previous values obtained by Brown et. al.[4] by IR laser spectroscopy in a very cold ($T_{rot} = 10$ K) supersonic jet.

Their rotational constants are included in Table IV and the comparison confirms the analysis of the fs Raman RCS experiments and our RCS fits. Small differences between the two sets of constants are to be expected, since we had to include centrifugal distortion constants in our non-rigid rotor fits at $T = 130$ and 293 K, while Brown et. al. could employ a rigid-rotor model at their low rotational temperatures.[4]

The supersonic-jet signal intensity was low, so only the most intense four J-type recurrences could be observed, as is shown in Figure 7. Although these recurrences do not yield very accurate rotational constants, we used them to check the room-temperature fitted $(A_0 + B_0)/2$. The supersonic-jet fitted $(A_0 + B_0)/2 = 4887(1)$ MHz agrees with the room-temperature fitted value of $(A_0 + B_0)/2 = 4884.5(7)$ MHz within the mutual 2σ values. The difference could be due to the poorer statistics of the analysis of the supersonic-jet transient, as well as to small errors of the calculated rotation-vibration coupling constants α_v^A, α_v^B, and α_v^C that were employed for the room-temperature gas-cell fit.

Figure 8 shows the experimental and simulated room-temperature gas cell RCS transient of p-dioxane-d_8. The 12 observed J and C-type transients allow for an determination of $(A_0+B_0)/2 = 4002.4(6)$ MHz and $C_0 = 2347.1(6)$ MHz with a similar accuracy as for p-dioxane-h_8, see Table IV. However, the individual rotational constants $A_0 = 4083(2)$ MHz and $B_0 = 3925(4)$ MHz of p-dioxane-d_8 have an almost 10x larger uncertainty than the combined constant $(A_0 + B_0)/2$. This again shows that transient complexity is much more important when determining rotational constants than transient length.

VI. THE STRUCTURE OF p-DIOXANE

By combining the experimentally measured rotational constants with the calculated equilibrium and vibrationally averaged rotational constants and the corresponding equilibrium structure parameters, it is possible to determine a semi-experimental equilibrium structure.[30–32,38,39,61,64] In short, we calculated the equilibrium r_e molecular structure and the equilibrium rotational constants A_e, B_e, C_e using the CCSD(T) method and Dunning's correlation-consistent core-valence polarized basis sets series cc-pCVXZ from double- to quadruple-zeta (X= D, T, Q). With the cc-pCVDZ basis set we additionally calculated the cubic force field necessary for the vibrational-averaging corrections $\Delta_A, \Delta_B, \Delta_C$ in eqn. (7). With our current computer resources, these could not be calculated with the larger (X=T,Q) basis sets, so we used the CCSD(T)/cc-pCVDZ values

in conjunction with all basis sets.

We generalized the previous two-point linear basis-set extrapolation method[38,39,61,64] to a three-point non-linear extrapolation, in which a CCSD(T) calculated vibrationally averaged rotational constant (e.g. A_0) is plotted vs. a given calculated equilibrium structure parameter of p-dioxane, [e.g. the equilibrium bond length r_e(C-C)]. Thus, for A_0 and r_e(C-C) which are calculated as a function of the basis-set size X, we plot $A_0 = C_1 + C_2 \cdot exp[C_3 \cdot r_e\text{(C-C)}]$. The semi-experimental r_e(C-C) bond length is obtained by extrapolating the calculated A_0/r_e(C-C) curve to the experimental A_0 value and determining the extrapolated r_e(C-C) value at the intersection. Analogous extrapolations are made for B_0/r_e(C-C) and C_0/r_e(C-C). The procedure is shown exemplarily in Figure 9 for the rotational constants A_0, B_0 and C_0 of p-dioxane-h_8 and the constants C_0 and $(A_0 + B_0)/2$ of p-dioxane-d_8, all of which are plotted vs. r_e(C-C). The experimental uncertainties of these five rotational constants are so small that they do not contribute significantly to the extrapolated r_e(C-C) values. However, the extrapolations yield slightly different values of r_e(C-C); Figure 9 shows that the spread for r_e(C-C) is 0.0009 Å and the corresponding 1σ is 0.0003 Å. We report the semi-experimental structure parameters in Table V as the average and $\pm 1\sigma$ standard deviation of the five values determined via the different rotational constants, e.g., r_e(C-C)$= 1.5135(3)$ Å.

Figure 9 also shows sub-plots involving the A_0 and B_0 constants of p-dioxane-d_8. Since these are ~ 10 times less precise than the other experimental constants, we did not include them in the analysis, but note that the respective extrapolated r_e(C-C) values are consistent with those of the other sub-plots. A further consistency check was done by comparing to the average rotational constant $(A_0 + B_0)/2$ of p-dioxane-h_8 (lower left in Figure 9), which gives r_e(C-C)$= 1.5136$ Å, in excellent agreement with the value above.

Previously we have employed linear two-point extrapolations using basis sets with $X = 2$ and 3.[38,39,61,64] Figure 9 now reveals that the extrapolation functions can be concave or convex, depending on the rotational constant. While our previous assumption of linearity is acceptable for some combinations of rotational constants and structure parameters, e.g, for $(A_0 + B_0)/2$ vs. r_e(C-C), it is clearly not valid for other combinations, e.g. A_0 or B_0 vs. r_e(C-C) bond length, see Figure 9.

The analogous plots for the semi-experimental equilibrium bond lengths r_e(C-O), r_e(C-H$_{eq}$), r_e(C-H$_{ax}$) and the equilibrium bond angles $\angle$C-O-C, $\angle$C-C-H$_{ax}$, $\angle$H-C-H and the flap angle are given in the supplemental Figures S2-S8 (see the SI); the corresponding semiexperimental struc-

ture parameters are collected in the fourth data column of Table V.

While the extrapolations in Figure 9 and Figures S2-S8 are *ordered* with respect to the basis-set size X, X is not a variable in this procedure, in contrast to usual basis-set extrapolation schemes. Thus, the extrapolation curve through the calculated points should approach the experimental rotational constant monotonically as a function of X and should not cross the experimental line; this is indeed observed in Figure 9 and Figures S2-S8 (in the SI). In general, the extrapolated semi-experimental structure parameters lie slightly beyond the CCSD(T)/cc-pCVQZ calculated values, indicating that the CCSD(T)/cc-pCVXZ combination is rather close to the basis-set limit. This has also been noted in several other studies.[39,45–47]

However, the condition of monotonicity is not fulfilled for the $\angle$(C-C-O) angle (Figure S9 in the SI) and for the $\angle$(C-C-H_{eq}) angle (not shown); the extrapolation procedure fails for these two structure parameters. The CCSD/pCVTZ and pCVQZ data columns of Table V indicate the approximate uncertainty of these two angles. Demaison et al. have noted similar problems when predicting semi-experimental bond angles and especially dihedral angles at the MP2/cc-pVTZ level.[30]

In Table V we list the extrapolated semi-experimental bond lengths and angles. The last two columns compare Raman RCS-based values to the gas-phase electron diffraction structure parameters r_α and r_a that are taken from ref. 7. These $T = 294$ K thermally averaged values[7] cannot be directly compared to the equilibrium structure parameters, since chemical bonds expand with increasing temperature and vibrational excitation.[65,66] Using CFOUR and the CCSD(T)/cc-pCVDZ cubic force field, we computationally converted the semi-experimental r_e values to the $r_a(294\text{ K})$ values, which are listed in the fifth data column of Table V. The uncertainties of the Raman RCS-based r_a values contain only the uncertainties of the semi-experimental r_e parameters, the errors of the computed force field are not known. The calculations predict that all bond lengths and angles increase with increasing temperature, except for the H-C-H bond angle and the flap angle. The semi-experimental Raman RCS r_a(C-H) bond lengths and bond angles are in good agreement with the GED values. However, the corresponding r_a(C-C) and r_a(C-O) bond lengths differ significantly, being 0.012 Å and 0.004 Å longer than the GED values; the flap angle differs by $0.9°$. While there might be contributions to these differences that arise from the CCSD(T)/cc-pCVDZ computed cubic force field, we believe that these differences are significant.

VII. DISCUSSION

The accurate semi-experimental structure of p-dioxane derived here allows interesting comparisons to the isoelectronic molecules piperidine and cyclohexane, whose equilibrium geometries are also chair-shaped. Their equilibrium semi-experimental structures have been determined by Demaison et. al. based on microwave spectroscopic data for piperidine[29,30] and deuterated cyclohexane isotopomers[25,26] using a mixed estimation method.[30] The semi-experimental equilibrium structure of cyclohexane has also been determined by combining Raman RCS spectroscopy of the h_{12} and $-d_{12}$ isotopomers with CCSD(T) calculations and basis-set interpolation.[27,28]

We first compare the semiexperimental C-C, C-N and C-O bond lengths: The r_e(C-C) bond distance of cyclohexane determined by Raman RCS is 1.5260 Å,[27,28] in excellent agreement with the $1.5258(6)$ Å value from microwave spectroscopy.[25,26,30] The r_e(C-N) bond distance in piperidine is $1.4589(2)$ Å[30] and the r_e(C-O) distance in p-dioxane is $1.4168(4)$ Å. The bond length decreases by 0.067 Å in piperidine and by 0.109 Å in p-dioxane relative to cyclohexane can be explained by the contraction of the valence orbitals of N and O due to the increased nuclear charge.[30]

When comparing the C-C bond distances along this series, one sees that the C2-C3 (and C5-C6) bond lengths in piperidine decrease to $1.5212(2)$ Å,[30] and the C2-C3 (and C5-C6) bonds in p-dioxane to $1.5135(3)$ Å, corresponding to contractions by 0.005 and 0.013 Å relative to cyclohexane. We interpret this as arising from a slight shrinkage of the sp^3-orbitals of the carbon atoms that are involved in the polar C-N and C-O bonds. That the shrinkage is larger in p-dioxane than in piperidine is in line with the larger polarity of the C-O bonds.

When comparing C-H bond lengths, we note that already in cyclohexane the semi-experimental $r_e(\text{C-H})_{ax} = 1.096$ Å is 0.004 Å longer than the equatorial C-H bond length $r_e(\text{C-H})_{eq}$.[25–28,30] A similar difference between the axial and equatorial C-H bond distances is found at the C4 atom of piperidine (the C atom farthest from the nitrogen). However, in piperidine the axial and equatorial C-H bond lengths at the C2 and C5 atoms differ by 0.012 Å. In p-dioxane the four axial C-H bond lengths are 0.008 Å longer than the four equatorial C-H bond lengths. In piperidine, these differences in equatorial and axial C-H bond lengths have been rationalized in terms of the *trans* effect,[30] in which a lone-pair (lp) at a heteroatom X that is chemically bound to a C-H group can delocalize into an antibonding σ^* orbital of this C-H bond, if the latter is oriented *trans* to this lone-pair (i.e., trans H-C-X-lp). In pyranose sugars, this is also referred to as the anomeric (or Edward-Lemieux) effect.[67–69]

VIII. CONCLUSIONS

We measured the femtosecond Raman rotational coherence transients of p-dioxane-h_8 and p-dioxane-h_8 in a gas-cell at $T = 293$ K. For p-dioxane-h_8 Raman RCS measurements were performed in a supersonic-jet experiment, allowing to cool the sample to $T_{rot} \sim T_{vib} \sim 130$ K. Fitting the experimental RCS transients to an asymmetric-top model allowed to determine the $v = 0$ ground-state rotational constants for p-dioxane-h_8 and p-dioxane-d_8. The RCS transient of p-dioxane-h_8 exhibits a number of A-, C-, and K-type asymmetry coherences that were analyzed using a sub-transient decomposition method,[61] allowing to separate coherences with specific rotational quantum number changes ($\Delta J = 0, 1, 2$ combined with $\Delta K = 0, 2$).

All of the coherences in the Raman RCS transient could be assigned to the most stable chair conformer of p-dioxane. No signals of the twist-boat conformer were observed by Raman RCS, confirming its very low concentration, in agreement with previous investigations using gas-phase electron diffraction.[2,7]

Perdeuteration of p-dioxane-h_8 changes the inertial tensor from a strongly asymmetric top ($\kappa = 0.66$) to a near-oblate symmetric top ($\kappa = 0.89$ for p-dioxane-d_8). This increase of symmetry leads to (1) a smaller number of asymmetry transients for the d_8-isotopomer as compared to the h_8 species, (2) an increase in the delay time over which recurrences can be observed i.e., $0-900$ ps for p-dioxane-d_8 as compared to $0-600$ ps for p-dioxane-h_8, and (3) to a decrease of the information content of the RCS spectrum, which results in $5-10$ times larger uncertainties of the A_0 and B_0 constants of p-dioxane-d_8 relative to those of p-dioxane-h_8.

Combining the experimentally determined rotational constants with CCSD(T)/cc-pCVXZ (X=D,T,Q) calculations allowed to determine accurate semi-experimental values for eight of the ten equilibrium structure parameters (bond lengths and angles). The exceptions are the C-C-O and C-C-H$_{eq}$ bond angles, which do not change monotonically when increasing the basis set from double- to quadruple-zeta. The semi-experimental equilibrium r_e(C-C) bond length is $1.5135(3)$ Å, which is $0.013(1)$ Å shorter than the value $1.526(1)$ Å determined for cyclohexane.[27,28] The four axial C-H bond lengths are determined to be r_e(C-H)$_{ax} = 1.096$ Å, which is 0.008 Å longer than the four equatorial C-H bond lengths. This difference is rationalized in terms of *trans* effect, which is also known as the *anomeric* effect in the context of pyranose sugars.[67–69]

We computationally converted the semi-experimental r_e values to the corresponding r_a values at $T = 294$ K for comparison to the gas-phase electron diffraction results. While most values are in

good agreement with those determined by gas-phase electron diffraction, [7] the thermally averaged r_a(C-C)$= 1.512(2)$ Å measured by GED does not agree well with the r_a(CC)$= 1.522$ Å that we compute based on our semi-experimental $r_e = 1.5135(3)$ Å value and the CCSD(T)/cc-pCVDZ cubic force field. We also note a 0.004 Å discrepancy between the computed/semi-experimental C-O distance $r_a = 1.4232(4)$ Å and the GED r_a value.[7]

Supplemental Material

See the Supplemental Material (SI) for an energy-level diagram of asymmetric top molecules, rotational Raman transient types, Z-matrices and CCSD(T) calculated structure parameters of the chair and twist-boat forms of p-dioxane, and eight Figures with additional semi-experimental structure parameter extrapolations.

Acknowledgments

This work has been supported by the Schweizerische Nationalfonds (SNSF) through grants No. 200020-144490 and 200020-130376.

---

* leutwyler@dcb.unibe.ch

[1] S. CHANDRAN and R. VARMA, *Spectrochim. Acta Part A* **153**, 704-708 (2015).

[2] M. DAVIS and O. HASSEL, *Acta Chem. Scand* **17**, 1181 (1963).

[3] F. A. L. ANET and J. SANDSTROM, *Chem. Comm.* **23**, 1558 (1971).

[4] P. R. BROWN and P. R. DAVIES, and G. M. HANSFORD, and N. A. MARTIN, *J. Mol. Spec.* **158**, 468-478 (1993).

[5] F. R. JENSEN and R. A. NEESE, *J. Am. Chem. Soc.* **93**, 6329 (1971).

[6] J. BUSCHMANN, E. MUELLER, and P. LUGER, *Acta Cryst.* **42**, 873 (1986).

[7] M. FARGHER, L. HEDBERG, and K. HEDBERG, *J. Mol. Struct.* **1071**, 41 (2014).

[8] P. M. FELKER and A. H. ZEWAIL, *J. Chem. Phys.* **86**, 2460 (1987).

[9] P. M. FELKER, *J. Phys. Chem.* **96**, 7844 (1992).

[10] P. M. FELKER and A. H. ZEWAIL, Molecular Structures from Ultrafast Coherence Spectroscopy, in *Femtosecond Chemistry*, edited by J. MANZ and L. WÖSTE, volume I, chapter 5, VCH, Weinheim, 1995.

[11] H.-M. FREY, P. BEAUD, T. GERBER, B. MISCHLER, P. P. RADI, and A. P. TZANNIS, *Appl. Phys. B* **68**, 735 (1999).

[12] H. M. FREY, P. BEAUD, T. GERBER, B. MISCHLER, P. P. RADI, and A. P. TZANNIS, *J. Raman Spectrosc.* **31**, 71 (2000).

[13] C. RIEHN, A. WEICHERT, and B. BRUTSCHY, *J. Phys. Chem. A* **105**, 5618 (2001).

[14] H. M. FREY, P. BEAUD, T. LANG, and M. MOTZKUS, High Resolution Femstosecond CARS Spectroscopy, in *Femtochemistry and Femtobiology: Ultrafast Dynamics in Molecular Science*, edited by A. DOUHAL and J. SANTAMARIA, chapter 1, p. 99, World Scientific Publishing, Singapore, 2002.

[15] H. M. FREY, A. MÜLLER, and S. LEUTWYLER, *J. Raman Spectrosc.* **33**, 855 (2002).

[16] P. HOBZA, C. RIEHN, A. WEICHERT, and B. BRUTSCHY, *Chem. Phys.* **283**, 331 (2002).

[17] V. V. MATYLITSKY, W. JARZEBA, C. RIEHN, and B. BRUTSCHY, *J. Raman Spectrosc.* **33**, 877 (2002).

[18] W. JARZEBA, V. V. MATYLITSKY, C. RIEHN, and B. BRUTSCHY, *Chem. Phys. Lett.* **368**, 680 (2003).

[19] C. RIEHN, V. V. MATYLITSKY, W. JARZEBA, B. BRUTSCHY, P. TARAKESHWAR, and K. KIM, *J. Am. Chem. Soc.* **125**, 16455 (2003).

[20] D. S. KUMMLI, H. M. FREY, M. KELLER, and S. LEUTWYLER, *J. Chem. Phys.* **123**, 054308 (2005).

[21] C. RIEHN, V. V. MATYLITSKY, M. F. GELIN, and B. BRUTSCHY, *Mol. Phys.* **103**, 1615 (2005).

[22] W. CAMINATI, A. D. ERBA, S. MELANDRI, and P. G. FAVARO, *J. Am .Chem. Soc* (1998).

[23] H. M. PICKETT and H. L. STRAUSS, *J. Am. Chem. Soc.* **92**, 7281 (1970).

[24] D. M. CHAPMAN and R. E. HESTER, *J. Phys. Chem. A* **101**, 3382 (1997).

[25] J. DOMMEN, T. BRUPBACHER, G. GRASSI, and A. BAUDER, *J. Am. Chem. Soc.* **112**, 953 (1990).

[26] E. BIAŁKOWSKA-JAWORSKA, M. JAWORSKI, and Z. KISIEL, *J. Mol. Struct.* **350**, 247 (1995).

[27] G. BRÜGGER, H.-M. FREY, P. STEINEGGER, F. BALMER, and S. LEUTWYLER, *J. Phys. Chem. A* **115**, 9567 (2011).

[28] G. BRÜGGER, H.-M. FREY, P. STEINEGGER, P. KOWALEWSKI, and S. LEUTWYLER, *J. Phys. Chem. A* **115**, 12380 (2011).

[29] H. EHRLICHMANN, J.-U. GRABOW, H. DREIZLER, N. HEINEKING, and M. ANDOLFATTO, *Z. Naturforsch., A* **44**, 841 (1989).

[30] J. DEMAISON, N. C. CRAIG, P. GRONER, P. ECIJA, E. J. COCINERO, A. LESARRI, and H. D. RUDOLPH, *J. Phys. Chem. A* **119**, 1486 (2015).

[31] J. DEMAISON, *Mol. Phys.* **105**, 3109 (2007).

[32] J. DEMAISON, H. D. RUDOLPH, and A. G. CSÁSZÁR, *Mol. Phys.* **111**, 1539 (2013).

[33] D. S. KUMMLI, H. M. FREY, and S. LEUTWYLER, *J. Chem. Phys.* **124**, 144307 (2006).

[34] D. S. KUMMLI, H. M. FREY, and S. LEUTWYLER, *Chimia* **60**, 212 (2006).

[35] D. S. KUMMLI, H. M. FREY, and S. LEUTWYLER, *J. Phys. Chem. A* **111**, 11936 (2007).

[36] D. S. KUMMLI, S. LOBSIGER, H. M. FREY, S. LEUTWYLER, and J. F. STANTON, *J. Phys. Chem. A.* **112**, 9134 (2008).

[37] A. C. ECKBRETH, *Appl. Phys. Lett.* **32**, 421 (1978).

[38] D. S. KUMMLI, H.-M. FREY, and S. LEUTWYLER, *Chem. Phys.* **367**, 36 (2010).

[39] T. S. DEN, H. M. FREY, and S. LEUTWYLER, *J. Chem. Phys.* **141**, 194303 (2014).

[40] C. G. VINSON and J. J. MARTIN, *J. Chem. Eng* **8**, 74 (1963).

[41] D. E. WOON and T. H. DUNNING JR., *J. Chem. Phys.* **103**, 4572 (1995).

[42] J. J. BARRETT and A. WEBER, *J. Mol. Spec.* **50**, 205 (1974).

[43] K. L. BAK, J. GAUSS, P. JØRGENSEN, J. OLSEN, T. HELGAKER, and J. F. STANTON, *J. Chem. Phys.* **114**, 6548 (2001).

[44] C. PUZZARINI, M. HECKERT, and J. GAUSS, *J. Chem. Phys.* **128**, 194108 (2008).

[45] C. PUZZARINI, J. F. STANTON, and J. GAUSS, *Int. Rev. Phys. Chem.* **29**, 273 (2010).

[46] C. PUZZARINI, *Phys.Chem. Chem. Phys* **15**, 6595 (2013).

[47] M. HOCHLAF, C. PUZZARINI, and M. SENENT, *Mol. Phys.* **113**, 1671 (2015).

[48] J. GAUSS and J. F. STANTON, *Chem. Phys. Lett.* **276**, 70 (1997).

[49] J. F. STANTON, C. L. LOPREORE, and J. GAUSS, *J. Chem. Phys.* **108**, 7190 (1998).

[50] CFOUR, a quantum chemical program package written by Stanton, J. F.; Gauss, J.; Harding, M. E.; Szalay, P. G.; with contributions from Auer, A. A.; Bartlett, R. J.; Benedikt, U.; Berger, C.; Bernholdt, D. E.; Bomble, Y. J.; Cheng, L.; Christiansen, O.; Heckert, M.; Heun, O.; Huber, C.; Jagau, T.-C.; Jonsson, D.; Jusélius, J.; Klein, K.; Lauderdale, W. J.; Matthews, D. A.; Metzroth, T.; O'Neill, D. P.; Price, D. R.; Prochnow, E.; Ruud, K.; Schiffmann, F.; Schwalbach, W.; Stopkowicz, S.; Tajti, A.; Vázquez, J.; Wang, F.; Watts, J. D. *and the integral packages MOLECULE* (Almlöf, J.; Taylor, P. R.), *PROPS* (Taylor, P. R.), *ABACUS* (Helgaker, T.; Jensen, H. J. Aa.; Jørgensen, P.; Olsen, J.), *and ECP routines by* Mitin, A. V.; van Wüllen, C. For the current version, see `http://www.cfour.de`.

[51] S. MUKAMEL, *Principles of Nonlinear Spectroscopy*, Oxford University Press, New York, 1995.

[52] B. GRIMBERG, V. LOZOVOY, M. DANTUS, and S. MUKAMEL, *J. Phys. Chem. A* **106**, 697 (2002).

[53] E. J. BROWN, Q. ZHANG, and M. DANTUS, *J. Chem. Phys.* **110**, 5772 (1999).

[54] G. PLACZEK and E. TELLER, *Z. Phys.* **81**, 209 (1933).

[55] W. GORDY and R. L. COOK, *Microwave Molecular Spectra*, Wiley-Interscience, New York, 3rd edition, 1984.

[56] J. K. G. WATSON, *Mol. Phys.* **15**, 479 (1968).

[57] C. H. TOWNES and A. L. SCHAWLOW, *Microwave Spectroscopy*, Dover Publications (reprint edn.), New York, 1975.

[58] D. A. LONG, *Raman Spectroscopy*, McGraw-Hill International Book Company, 1977.

[59] H. W. KROTO, *Molecular Rotation Spectra*, Dover Publications, Inc. New York, 1992.

[60] D. A. LONG, *The Raman Effect: A Unified Treatment of the Theory of Raman Scattering by Molecules*, John Wiley & Sons, Ltd, 2002.

[61] T. S. DEN, H. M. FREY, P. M. FELKER, and S. LEUTWYLER, *J. Chem. Phys.* **143**, 144306 (2015).

[62] P. JOIREMAN, L. C. CONNELL, S. M. OHLINE, and P. M. FELKER, *J. Chem. Phys.* **96**, 4118 (1992).

[63] G. HERZBERG, *Molecular Spectra and Molecular Structure: III. Electronic Spectra and Electronic Structure of Polyatomic Molecules*, D. Van Nostrand Company, 1966.

[64] P. KOWALEWSKI, H.-M. FREY, D. INFANGER, and S. LEUTWYLER, *J. Phys. Chem. A* **119**, 11215 (2015).

[65] A. DOMENICANO and I. HARGITTAI, editors, *Accurate Molecular Structures: Their Determination and Importance*, Oxford University Press, 1992.

[66] J. R. DURIG, *Equilibrium Structural Parameters*, volume 24, Elsevier, Amsterdam, 2000.

[67] J. T. EDWARD and I. PUSKAS, *Can. J. Chem.* **40**, 711 (1961).

[68] R. U. LEMIEUX and A. R. MORGAN, *Can. J. Chem.* **43**, 2205 (1965).

[69] S. WOLFE, A. RAUK, L. M. TEL, and I. G. CZISMADIA, *J. Chem. Soc.(B)* **1**, 136 (1971).

TABLE I. CCSD(T) calculated equilibrium and v=0 vibrationally averaged rotational constants (in MHz), A-reduced centrifugal distortion constants (in kHz) and molecular polarizability tensor components (in atomic units) of p-dioxane(-h_8, and -d_8) of the chair conformation and of the twist-boat conformation of p-dioxane-h_8 .

	chair-h_8			chair-d_8			twist-boat-h_8	
	cc-pCVDZ	cc-pCVTZ	cc-pCVQZ	cc-pCVDZ	cc-pCVTZ	cc-pCVQZ	cc-pCVDZ	cc-pCVTZ
	Rotational constants / MHz							
A_e	5094.23	5137.48	5142.90	4036.70	4094.11	4114.13	5151.27	5195.65
B_e	4635.52	4698.16	4723.65	3920.90	3960.52	3965.51	4484.10	4556.92
C_e	2737.84	2763.36	2771.66	2339.63	2362.56	2368.98	2790.76	2826.38
A_0	5035.77	5079.02[a]	5084.44[a]	4000.61	4085.02[a]	4078.04[a]	5086.92	5131.30[a]
B_0	4593.20	4655.84[a]	4681.33[a]	3880.14	3919.76[a]	3924.75[a]	4444.94	4517.76[a]
C_0	2708.88	2734.40[a]	2742.70[a]	2316.46	2339.39[a]	2345.81[a]	2757.32	2792.94[a]
κ [b]	0.620	0.639	0.656	0.857	0.811	0.823	0.449	0.475
	Centrifugal distortion constants / kHz							
Δ_J	1.2474			0.6773			1.1766	
Δ_K	1.1465			0.4065			0.9345	
Δ_{JK}	-2.1886			-0.9402			-1.8157	
δ_J	0.01065			-0.0364			-0.0606	
δ_K	1.3919			0.0591			0.6596	
	Polarizability tensor elements / bohr^3							
α_{aa}	54.8			54.7			42.5	
α_{bb}	42.8			42.9			53.8	
α_{cc}	43.4			43.3			43.2	
α_{ab}	0.0			0.0			0.0	
α_{ac}	0.0			0.0			0.0	
α_{bc}	1.10			1.10			0.0	
$\alpha^{(2)}_{(0)}$	-4.45			-4.49			-4.04	
$\alpha^{(2)}_{(1)}$	-1.10			-1.08			0.0	
$\alpha^{(2)}_{(2)}$	-5.95			-5.90			-5.65	
$\alpha^{(2)}_{(0)}/\alpha^{(2)}_{(2)}$	0.75			0.76			0.72	

[a] Calculated using the cc-pCVDZ Δ_A, Δ_B and Δ_C values where e.g. $\Delta_B = B_e - B_0$.

[b] $\kappa = \frac{2B-A-C}{A-C}$ is a measure of the asymmetry of a molecule where a value of +1 corresponds to an oblate symmetric-top and a value of -1 corresponds to a prolate symmetric-top.

TABLE II. The relationship of the irreducible spherical polarizability components $\alpha_k^{(j)}$ to their molecular polarizability Cartesian counterparts $\alpha_{\rho\sigma}$, from ref. 60. For p-dioxane $\alpha_{zz} = \alpha_{cc}$, $\alpha_{yy} = \alpha_{aa}$ and $\alpha_{xx} = \alpha_{bb}$.

ΔJ	ΔK	$\alpha_k^{(j)}$	$\alpha_{\rho\sigma}$
	2	$\alpha_2^{(2)}$	$\frac{1}{2}[(\alpha_{xx} - \alpha_{yy}) + i(\alpha_{xy} + \alpha_{yx})]$
± 2	1	$\alpha_1^{(2)}$	$-\frac{1}{2}[(\alpha_{xz} + \alpha_{zx}) + i(\alpha_{yz} + \alpha_{zy})]$
± 1	0	$\alpha_0^{(2)}$	$\frac{1}{\sqrt{6}}(2\alpha_{zz} - (\alpha_{xx} + \alpha_{yy}))$
0	-1	$\alpha_{-1}^{(2)}$	$\frac{1}{2}[(\alpha_{xz} + \alpha_{zx}) - i(\alpha_{zy} + \alpha_{yz})]$
	-2	$\alpha_{-2}^{(2)}$	$\frac{1}{2}[(\alpha_{xx} - \alpha_{yy}) - i(\alpha_{xy} + \alpha_{yx})]$

TABLE III. CCSD(T)/cc-pCVDZ calculated vibrational frequencies of p-dioxane-h_8 and p-dioxane-d_8 (in cm^{-1}) up to ν_{12}, relative vibrational populations and relative signal intensities (in %) at 298 K and 130 K and calculated rotation-vibration constants $\alpha_v^{A,B,C}$ (in MHz).

		T=298 K		T=130 K		α_v^A	α_v^B	α_v^C
Normal Mode	Wave Number	Population	Signal	Population	Signal			
			p-**dioxane**-h_8					
$v=0$	0.0	37.7	82.7	98.7	99.4			
ν_7	266.3	10.4	6.3	5.4	0.4	1.56	5.08	3.39
ν_8	279.6	9.8	5.6	3.9	0.2	9.61	-0.55	-0.74
ν_9	433.5	4.6	1.3	0.8	0.0	6.61	35.20	3.14
ν_{10}	445.7	4.4	1.1	0.6	0.0	7.47	-38.36	12.33
ν_{11}	487.5	3.6	0.7	0.4	0.0	-8.96	2.34	-9.38
ν_{12}	615.8	1.9	0.2	0.1	0.0	-0.05	3.02	2.63
$2\nu_7$	532.6	2.9	0.5	0.3	0.0			
$2\nu_8$	559.1	2.5	0.4	0.2	0.0			
ν_7+ν_8	545.9	2.7	0.4	0.2	0.0			
			p-**dioxane**-d_8					
$v=0$	0.0	26.3	71.0	78.9	98.2			
ν_7	196.1	10.2	10.7	9.0	1.3	3.59	1.09	2.00
ν_8	243.9	8.1	6.7	5.3	0.4	-0.24	5.64	0.36
ν_9	350.3	4.8	2.4	16.	0.0	9.46	5.71	3.79
ν_{10}	407.1	3.7	1.4	0.9	0.0	2.07	-2.89	14.29
ν_{11}	421.4	3.4	1.2	0.7	0.0	-10.70	-0.38	-13.79
ν_{12}	483.3	2.6	0.7	0.4	0.0	2.70	-0.83	1.54
$2\nu_7$	392.2	4.0	1.6	1.0	0.0			
$2\nu_8$	487.8	2.5	0.6	0.4	0.0			
ν_7+ν_8	404.0	3.1	1.0	0.6	0.0			

TABLE IV. Experimental and CCSD(T) calculated ground state rotational constants of p-dioxane-h_8 and p-dioxane-d_8 (in MHz, $\pm 1\sigma$ uncertainties in parentheses).

	p-dioxane-h_8				p-dioxane-d_8	
Constant	CCSD(T)/ cc-pCVQZ [a]	fs-Raman RCS supers. jet	fs-Raman RCS gas-cell	IR Diode laser jet [b]	CCSD(T)/ cc-pCVQZ [a]	fs-DFWM gas-cell [b]
A_0	5084.44		5084.4(5)	5083.2(3)	4078.04	4083(2)
B_0	4681.33		4684(1)	4684.4(3)	3924.75	3925(4)
C_0	2742.70		2744.7(8)	2743.6(1)	2345.81	2347.1(6)
$(A_0 + B_0)/2$	4882.885	4887(1)	4884.5(7)	4883.8(3)	4001.395	4002.4(6)

[a] Calculated using the cc-pCVDZ Δ_A, Δ_B and Δ_C values where e.g. $\Delta_B = B_e - B_0$.

[b] Ref. 4, fit without centrifugal distortion constants, see eqn. (4).

TABLE V. CCSD(T) calculated, and semi-experimental bond lengths (in Å) and bond angles (in degrees) for p-dioxane. $\pm 1\sigma$ uncertainties in parentheses. Experimental $r_{\alpha,294\mathrm{K}}$ and $r_{\mathrm{a},294\mathrm{K}}$ bond lengths and bond angles from ref. 7 are given in the last two columns.

	r_{e}CCSD(T)			r_{e}	r_{a}	r_{α}	r_{a}
	pCVDZ	pCVTZ	pCVQZ	fs-Raman	RCS	GED, ref. 5	
Bond length							
r(C-C)	1.5267	1.5154	1.5139	1.5135(3)	1.5221(3)	1.510(2)	1.512(2)
r(C-O)	1.4254	1.4191	1.4172	1.4168(4)	1.4232(4)	1.417(1)	1.419(1)
r(C-H$_{eq}$)	1.1037	1.0892	1.0886	1.0885(1)	1.0935(1)	1.082(2)	1.094(2)
r(C-H$_{ax}$)	1.1120	1.0971	1.0964	1.0963(1)	1.1016(1)	1.090(2)	1.102(2)
Bond angle							
$\angle$ C-O-C	109.292	109.618	109.907	110.1(1)	110.5(1)	110.9(5)	110.7(5)
$\angle$ C-C-O	110.556	110.621	110.556	[a]	110.6 [b]	111.1(2)	110.9(2)
$\angle$ C-C-H$_{eq}$	110.964	110.859	110.898	[a]	110.9 [b]	106.9(28)	
$\angle$ C-C-H$_{ax}$	109.142	109.411	109.474	109.481(7)	109.553(7)	104.6(28)	
$\angle$ H-C-H	108.990	109.067	109.118	109.123(5)	108.989(5)	108.0(13)	
flap [c]	52.639	52.331	52.305	52.299(6)	51.924(6)	50.6(4)	51.1(4)

[a] The $\angle$ C-C-O and $\angle$ C-C-H$_{eq}$ angles do not extrapolate monotonically with increasing basis-set size (see the text).

[b] The CCSD(T)/cc-pCVQZ calculated values were used for the estimation of $r_{a,294K}$

[c] The angle between the COC plane and the plane of the four carbon atoms.

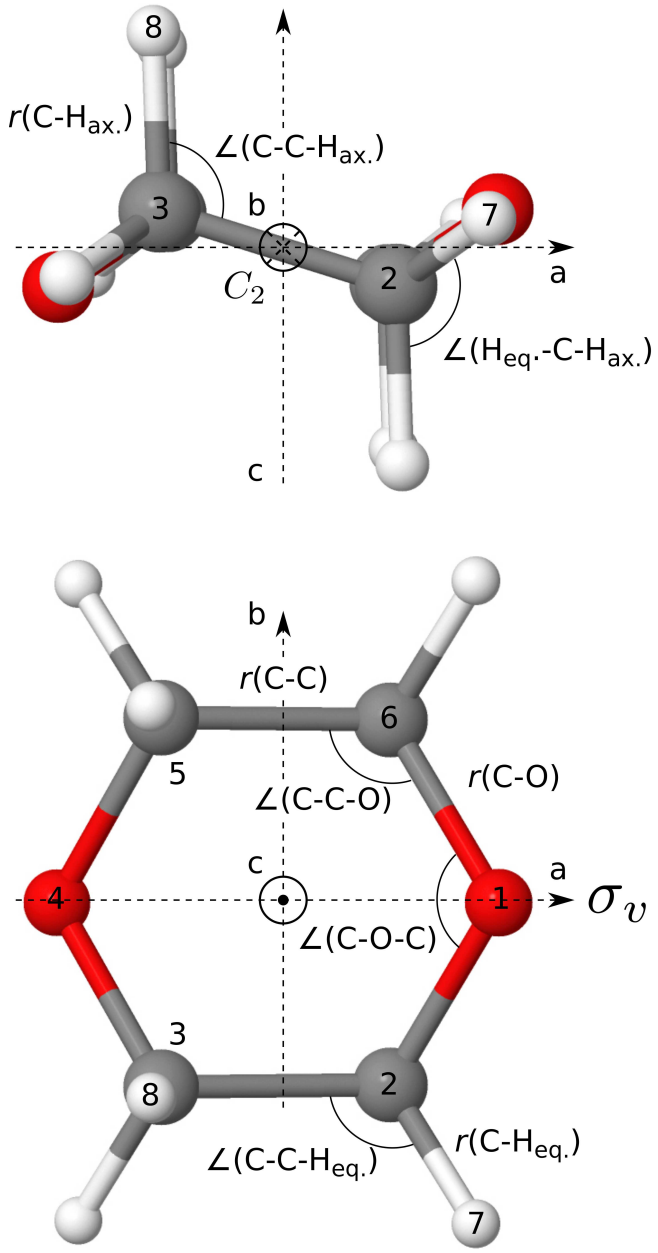

FIG. 1. Equilibrium structure of p-dioxane and definition of nine of the ten structure parameters. The inertial $\{a, b, c\}$ axes are indicated by dashed lines ($\otimes$ and $\bullet$ indicate down- and up-pointing axes respectively). Also indicated are the C_2 and $sigma_h$ symmetry operations of the C_{2h} point group.

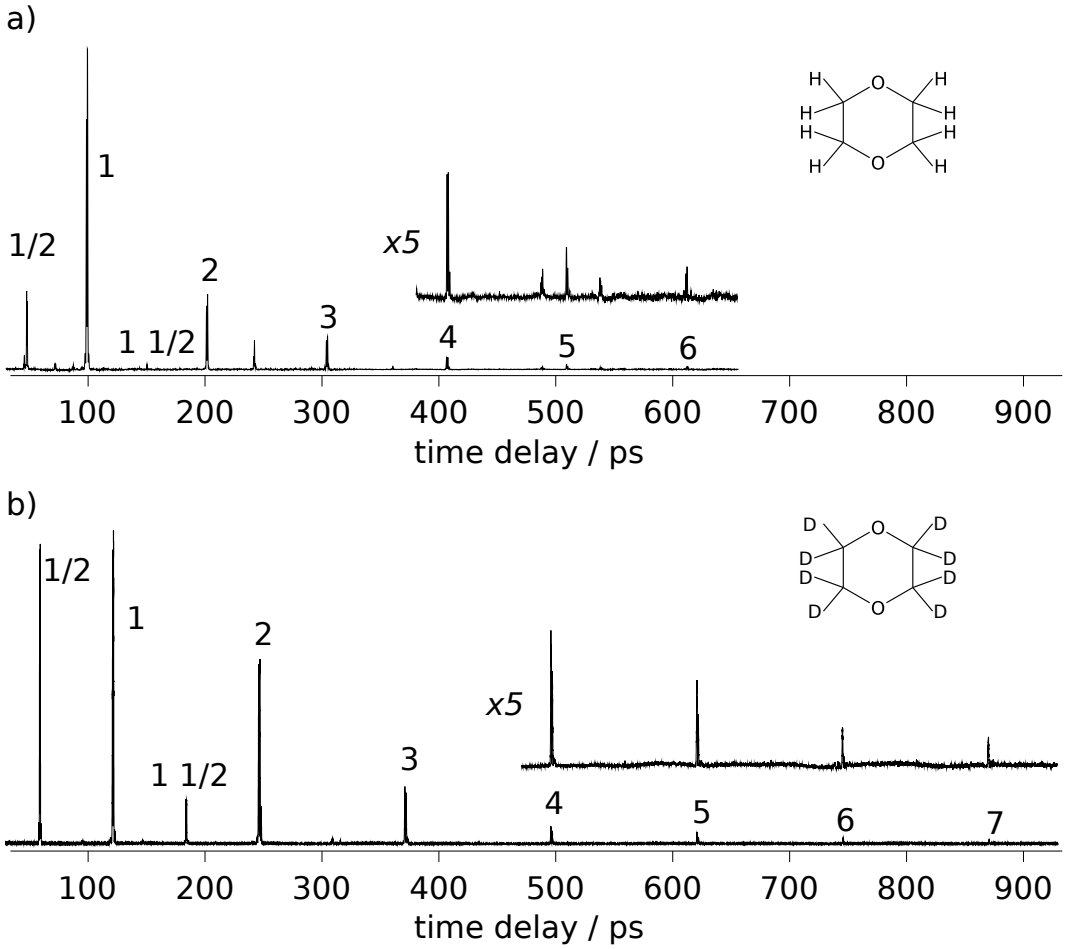

FIG. 2. Raman RCS transients of p-dioxane-h_8 and p-dioxane-d_8, measured in a gas cell at $T = 293$ K and $p = 30$ mbar.

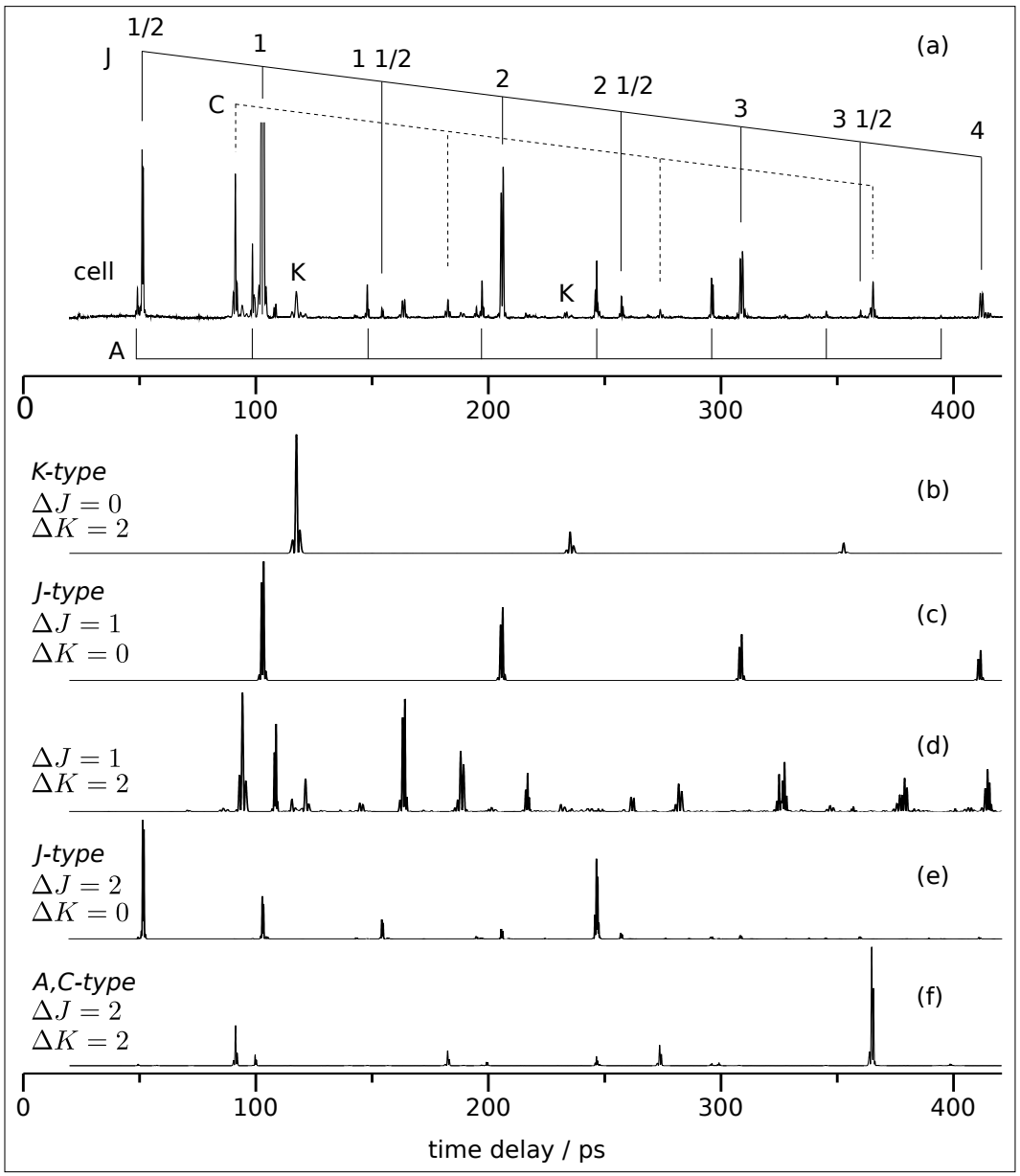

FIG. 3. Detailed assignment of the $T = 293$ K gas-cell Raman RCS transient of p-dioxane-h_8 for time delays t =0-400 ps: (a) Magnified and assigned experimental fs Raman RCS transient. (b) - (f) Sub-transients that simulated by restricting the coherences to Raman-allowed $\Delta J, \Delta K$ transitions.

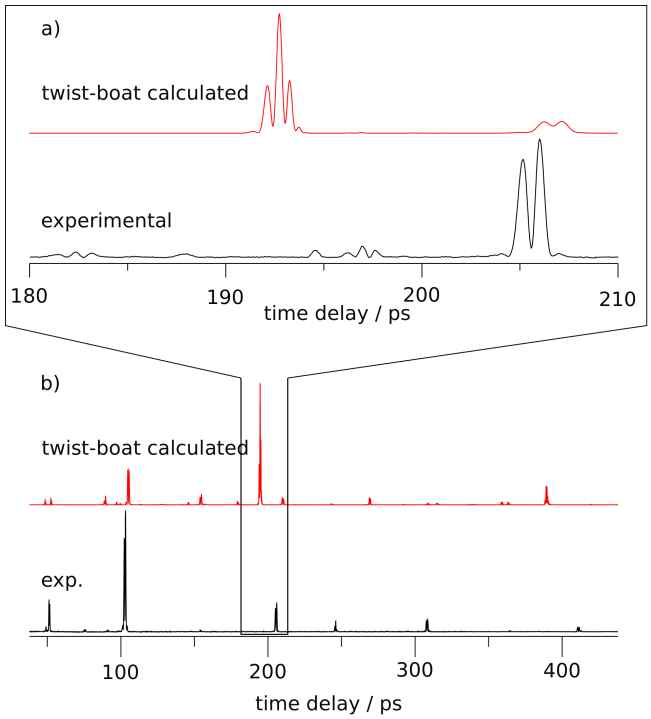

FIG. 4. Experimental room-temperature RCS transient of $para$-dioxane, compared to the calculated RCS transient of the twist-boat conformer. Panel (b) shows the experimental and calculated RCS transients for $t = 50 - 450$ ps. The most intense simulated coherences of the twist-boat conformer are magnified horizontally and compared to the experiment in panel (a).

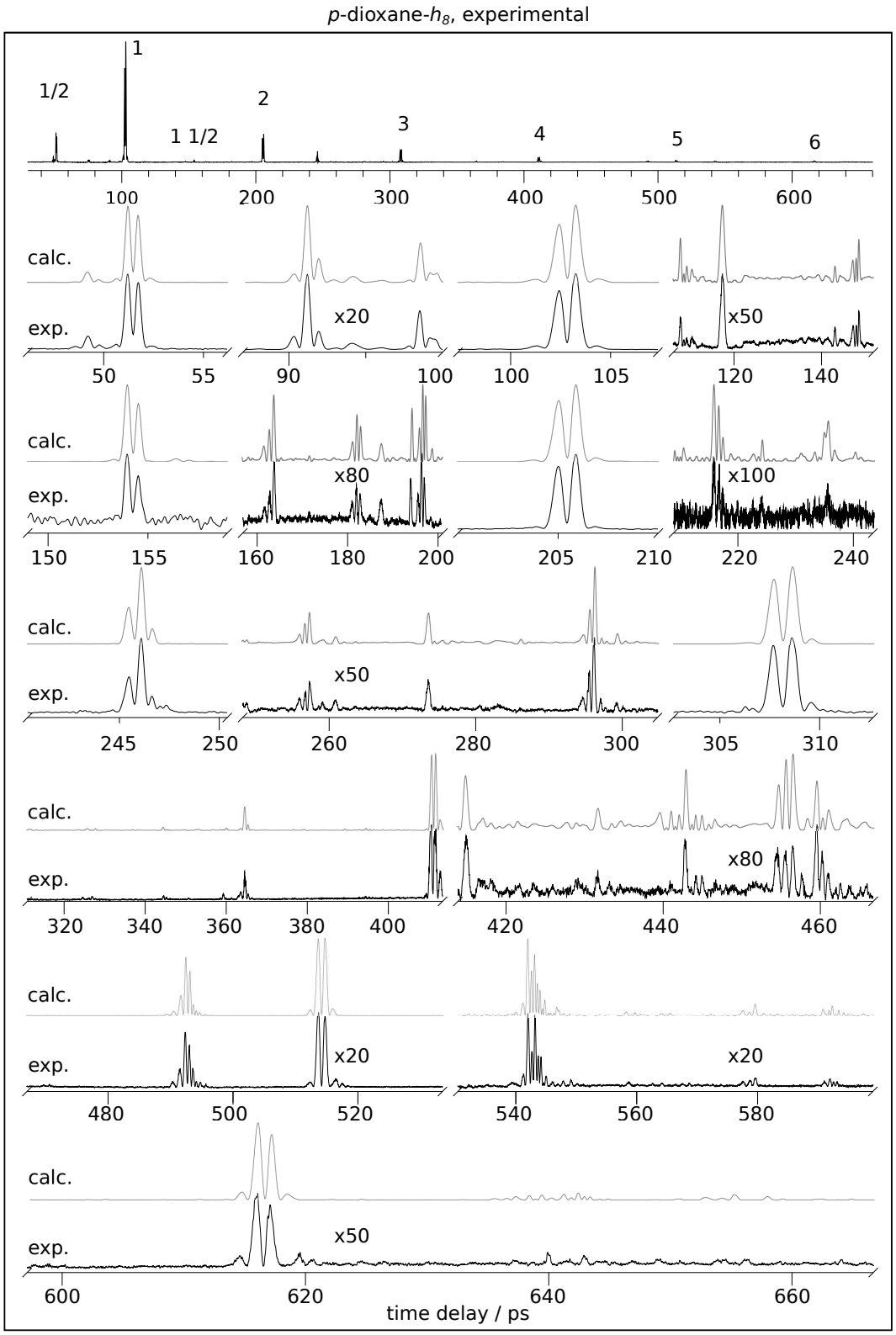

FIG. 5. Experimental and simulated femtosecond rotational Raman RCS spectrum of p-dioxane-h_8 in a room-temperature gas cell for delay time $t = 50 - 670$ ps. The fine structure is well reproduced by the simulation upon including signal contributions from the low-lying vibrational levels ν_7, ν_8, ν_9, ν_{10}, ν_{11}, ν_{12}, $2\nu_7$, $2\nu_8$ and ν_7+ν_8, see also Table III.

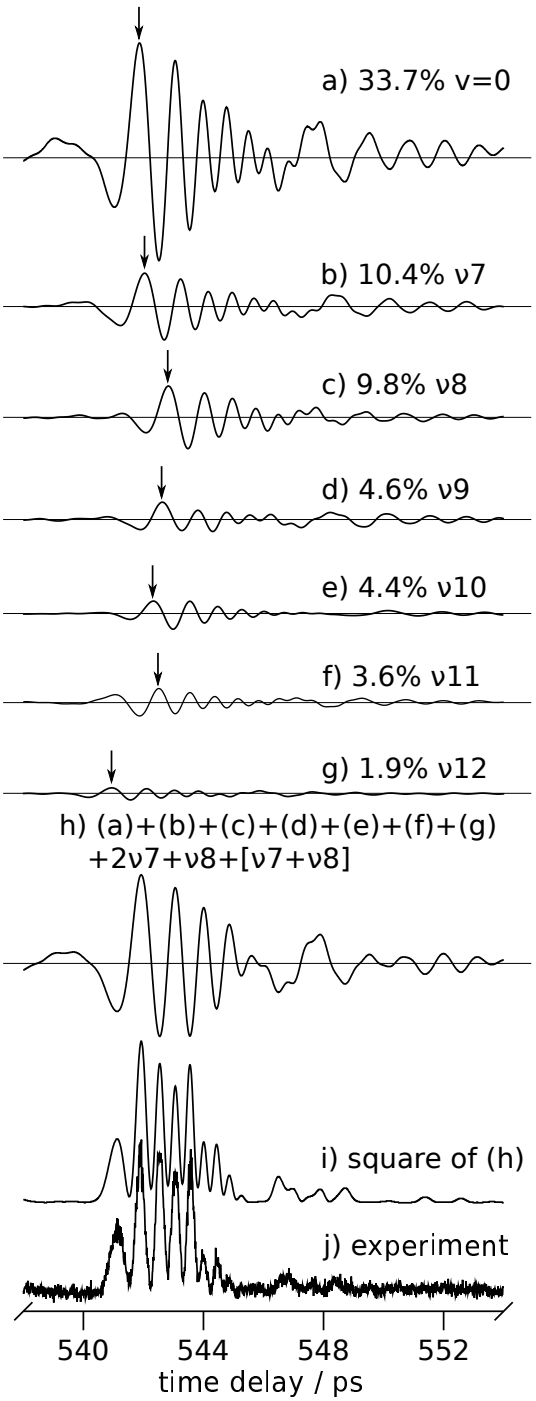

FIG. 6. The calculated $\chi^{(3)}(t)$ contributions to eqn.(2) for $\Delta t = 538 - 554$ ps at $T = 293$ K from (a) the $v = 0$ vibrational level and (b) - (g) the $v = 1$ levels of modes $\nu_7 - \nu_{12}$. The vertical arrows mark the positive maximum of the contributions to $\chi^{(3)}$. These are shifted relative to the trace (a) due to their slightly different rotational constants A_v, B_v, C_v, see eqns.(6) and (7). Trace (h) shows the summed contributions from (a)-(g) plus the contributions from the overtone levels $2\nu_7$, $2\nu_8$ and the $\nu_1 + \nu_2$ combination; see also Table III. Trace (i) gives the modulus-square of $\chi^{(3)}(t)$, see eqns.(1) and (2), which is compared to the experimental signal $I_{DFWM} \sim |\chi^{(3)}|^2$.

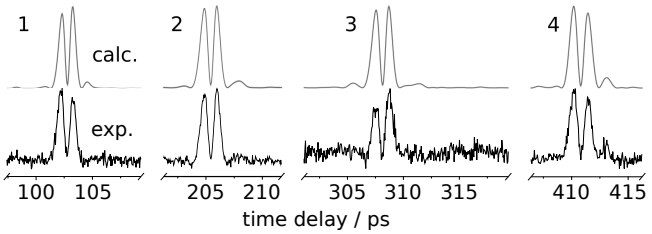

FIG. 7. Experimental and simulated femtosecond Raman RCS transient of p-dioxane-h_8 in an Ar supersonic-jet at $T_{rot} = T_{vib} = 130$ K.

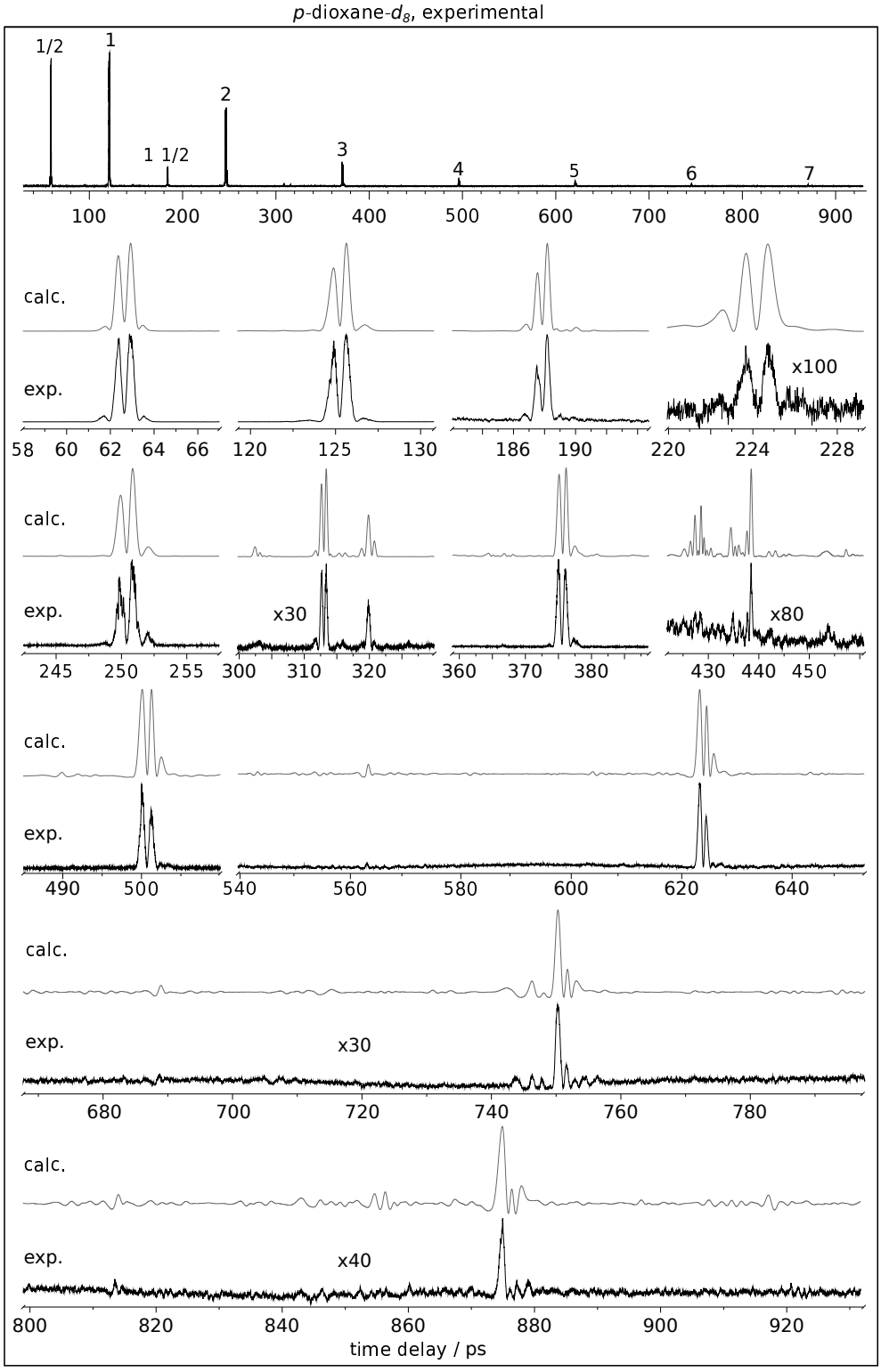

FIG. 8. Experimental and simulated femtosecond rotational Raman RCS spectrum of p-dioxane-d_8 in a room-temperature gas cell for delay time $t = 60 - 920$ ps. Low-lying vibrational levels ν_7, ν_8, ν_9, ν_{10}, ν_{11}, ν_{12}, $2\nu_7$, $2\nu_8$ and ν_7+ν_8 were included in the fit, see also Table III.

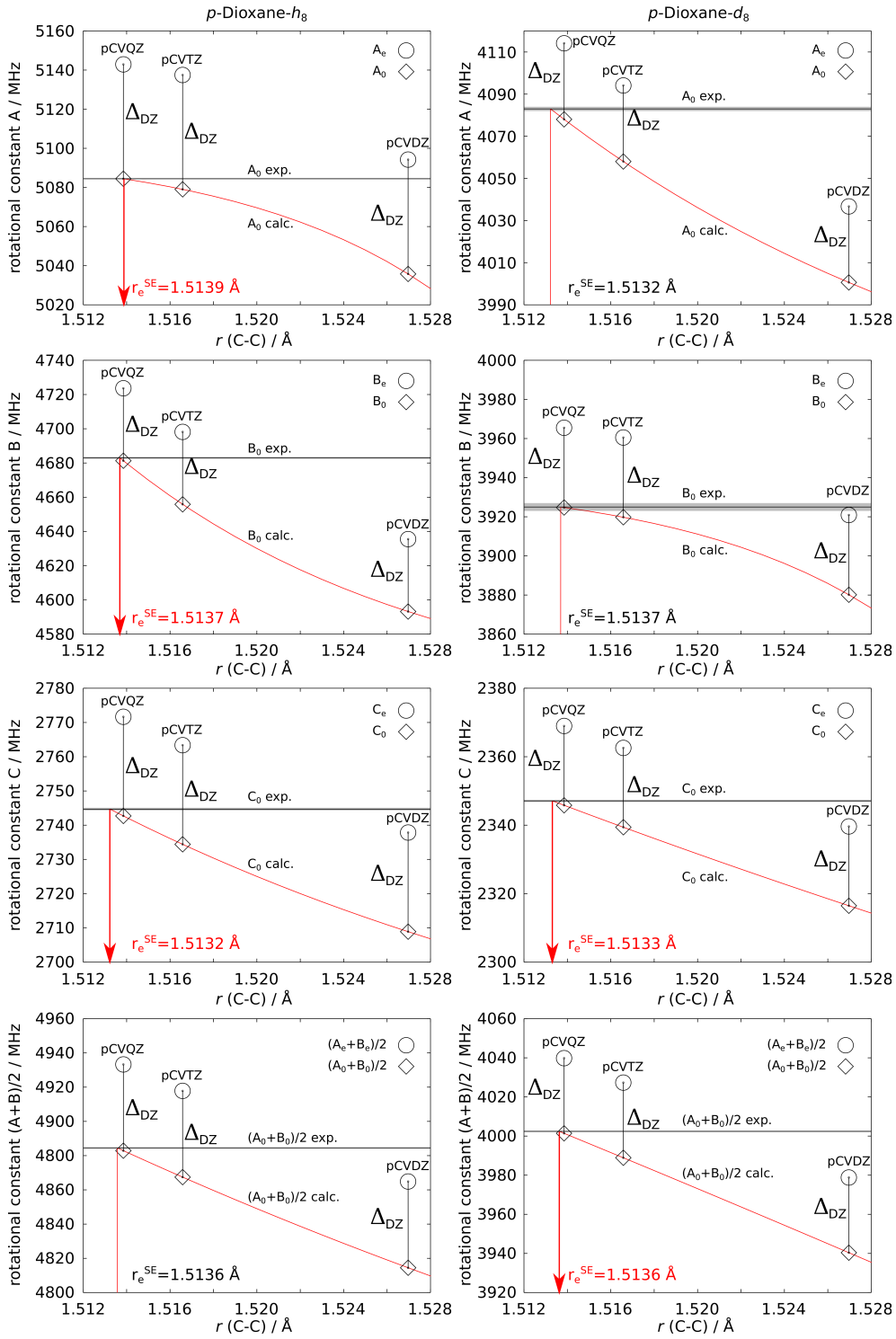

FIG. 9. CCSD(T) calculated equilibrium rotational constants (◯) and vibrational ground state rotational constants (◇) of p-dioxane, plotted vs. the equilibrium r_e(C-C) bond length. The extrapolated vibrational ground state rotational constants are connected by red lines. The semi-experimental r_e^{SE}(C-C) bond length is determined by intersecting the extrapolation function with the experimental rotational constant (drawn as horizontal black lines). This procedure is shown for the rotational constants $A_0, B_0, C_0, (A_0 + B_0)/2$ of p-dioxane-h_8 (left) and p-dioxane-d_8 (right).